Geomechanics for Energy and the Environment 43 (2025) 100697

Contents lists available at ScienceDirect

Geomechanics for Energy and the Environment

journal homepage: www.elsevier.com/locate/gete

Numerical study of the effect of soil-plant-atmosphere interaction under future climate projections and different vegetation covers

Maryam Sadat Maddah Sadatieh [a,b,*], Aikaterini Tsiampousi [a], Athanasios Paschalis [a,c]

[a] Imperial College London, Department of Civil and Environmental Engineering, London, UK
[b] Science and Solutions for a Changing Planet DTP, Grantham Institute, London, UK
[c] University of Cyprus, Department of Civil and Environmental Engineering, Nicosia, Cyprus

A R T I C L E I N F O

Keywords:
Soil-plant-atmosphere interaction
Vegetation
Safety
Numerical modelling
Climate projections

A B S T R A C T

Soil-plant-atmosphere interaction (SPAI) plays a significant role on the safety and serviceably of geotechnical infrastructure. The mechanical and hydraulic soil behaviour varies with the soil water content and pore water pressures (PWP), which are in turn affected by vegetation and weather conditions. Focusing on the hydraulic reinforcement that extraction of water through the plant roots offers, this study couples advances in ecohydrological modelling with advances in geotechnical modelling, overcoming previous crude assumptions around the application of climatic effects on the geotechnical analysis. A methodology for incorporating realistic ecohydrological effects in the geotechnical analysis is developed and validated, and applied in the case study of a cut slope in Newbury, UK, for which field monitoring data is available, to demonstrate its successful applicability in boundary value problems. The results demonstrate the positive effect of vegetation on the infrastructure by increasing the Factor of Safety. Finally, the effect of climate change and changes in slope vegetation cover are investigated. The analysis results demonstrate that slope behaviour depends on complex interactions between the climate and the soil hydraulic properties and cannot be solely anticipated based on climate data, but suctions and changes in suction need necessarily to be considered.

1. Introduction

A large part of the engineering infrastructure (railways, highways etc.) is comprised of earthwork slopes. In the UK alone, there are about 20,000 km of embankments and cuttings.[1,2] Infrastructure slope failures can be highly dangerous for the safety of the public. Furthermore, they affect the performance of the railway or highway they support, with significant socioeconomic and financial impacts, complete route closures or delays, and need for urgent mitigation. As an indication of the financial cost, Network rail spent £ 1.9 billion on maintenance in 2021–2022.[3] In addition to slope failures, deformations and displacements above serviceability limits can also have negative socioeconomic impacts due to imposed speed limits and delays.[4]

Geotechnical infrastructure is negatively affected by climate change,[5,6] with general trends of higher temperatures, varying patterns of precipitation change, a global increase in intense rainfall events, and rise in sea water levels,[6–9] affecting slope stability and serviceability through ground water table and Pore Water Pressure (PWP) variations.[10] These are specifically pronounced in shallow depths where interaction with the atmosphere is critical.[11] One of the leading reasons for slope failure is the reduction of tensile PWPs (suctions) near the slope surface or the rise in ground water table and associated increase of compressive PWPs, which reduce the soil's effective stress and therefore shear strength, while increasing the soil unit weight and the applied shear stresses.[12] Furthermore, seasonal water content changes due to soil-plant-atmosphere interaction (SPAI) cause soil volume changes, i.e. seasonal shrinking and swelling, markedly reducing the serviceability of infrastructure slopes.[13]

Due to its complexity, it is advantageous to simulate the effect of SPAI on the factor of safety and displacements of infrastructure slopes numerically, rendering climatic Boundary Conditions (BC) critical in geotechnical analysis. Various simplifications have been followed in the literature, such as imposing pre-defined winter and summer PWP profiles[14,15], or calculating PWP in flow analyses separately from the corresponding stresses, and applying them in stability analyses in non-coupled approaches.[16] More recently, fully coupled analyses were conducted, where the boundary conditions were derived from untreated weather data of rainfall and crude estimates of evapotranspiration,

* Correspondence to: Imperial College London, Exhibition Rd., South Kensington, London SW7 2AZ, UK.
E-mail address: m.maddah-sadatieh22@imperial.ac.uk (M.S. Maddah Sadatieh).

https://doi.org/10.1016/j.gete.2025.100697
Received 12 November 2024; Received in revised form 20 May 2025; Accepted 3 June 2025
Available online 4 June 2025

Fig. 1. Cut slope located in Newbury covered by grass and shrub.

overly simplifying complex interactions between the soil, the plants and the atmosphere.[17–20]

The complexity partly arises from the fact that, although rainfall is widely measured with weather stations, evapotranspiration (ET) is rarely measured and is commonly approximated by potential evapotranspiration (PET), which refers to the maximum amount of water extraction that can potentially occur if soil water supply is unlimited.[21–24] It is commonly calculated using the physically based Penman-Monteith method[25], or some variation of it, or, when data are limited, using empirical formulae, such as Thornthwaite's equation.[26]

As PET refers essentially to ideal conditions of infinite water supply in the ground, there have been attempts to estimate and apply the Actual Evapotranspiration (AET), i.e., the evapotranspiration that actually occurs considering water availability. To obtain the actual from the potential evapotranspiration, the relationship introduced by Feddes et al.[27] has been commonly used: it introduces a dimensionless multiplicative reduction term, which depends on head or suction. Low AET values occur when either anaerobic conditions or drought limit actual plant transpiration and soil evaporation.[17,28]

Alternatives to the Feddes et al. approach have been sought. Albino et al. used Wilson et al.'s[29] method to calculate AET with a coefficient that is a function of not only suction, as in Feddes et al., but also temperature.[30] Rather than employing a reduction term, Jamalinia et al. estimated AET using a crop model for grass that could account for vegetation growth in water limited conditions.[18] The net water entering the root zone in the crop model was then applied as a top boundary condition in a geotechnical model in which the hydraulic properties of the root zone were back-calculated to produce the same drainage from the bottom of the root zone as in the crop model. Rather than considering AET directly in their geotechnical analysis, Rouainia et al. used a hydrological model to obtain daily near surface PWPs which were subsequently applied as a boundary condition in a fully coupled hydro-mechanical finite difference analysis to investigate progressive failure on the Newbury cut slope under synthetic control of future climate projections.[31]

Previous attempts simplified the interplay of soil water availability, actual plant transpiration and plant growth. Therefore, in contrast to previous studies, in this paper, the physically based ecohydrological model Tethys – Chloris (T&C)[32,33] was used. T&C calculates actual evapotranspiration directly and integrates both water limited and energy limited approaches, coupling water, carbon and energy cycles at the soil surface and providing a detailed approach to vegetation processes. It simulates in detail plant physiological responses to environmental forcing, such as plant stomata regulation and plant growth, and based on that, it dynamically predicts realistic plant water use and actual soil water evaporation. This far exceeds the simplistic formulations so far used to define this important boundary condition in previous geotechnical work.

In the present work, the AET rates calculated by the ecohydrological T&C model were applied directly to a geotechnical Finite Element model in PLAXIS 2D[34] without any manipulation, obtaining a reliable estimate of the boundary condition. This is in contrast to previous studies, where either AET was roughly estimated through empirical coefficients or PET, which was calculated with simplistic assumptions, was used instead of accurately calculated AET rates. As unrealistic rates can have a significant effect on the calculated PWP in the geotechnical analysis, and by extension on soil behaviour and slope stability and serviceability, employing for the first time dynamically calculated AET in a geotechnical assessment is a significant advancement in the application of SPAI in geotechnical engineering. The T&C and PLAXIS computed PWP were in good agreement without the need to manipulate any of the soil properties or directly control the generated PWP, as in previous studies, successfully coupling for the first time advanced ecohydrological modelling with advanced geotechnical modelling. Good agreement was also observed between the computed and field measured suctions for a slope located in Newbury, UK. To quantify the impact of climate change through vegetation dynamics on factors of safety and slope serviceability, a geotechnical risk assessment was conducted considering multiple climate change projections. The analyses results were interrogated for evidence of correlations between climatic data and slope behaviour and the irreplaceable role of field PWP and displacement monitoring was corroborated.

2. Modelling approach

A three-step modelling strategy was followed:

(a) an ecohydrological model (T&C) able to capture both the water flow in and out of the soil under the effect of variable weather conditions and seasonal vegetation growth was run first for a representative column of soil.

(b) The T&C computed net inflow/outflow rates were then applied as a surface boundary condition in a 2D geotechnical model of a cut slope in PLAXIS 2D and the numerical results were validated against existing field measurements of variations of PWP with depth at different time instances and different locations.

(c) Climate projections were applied to the validated 2D model of the slope, considering two representative vegetation covers.

2.1. Case study

The selected case study is a cut slope in Newbury, UK (UK Ordnance Survey grid reference SU455652 – (latitude, longitude) = (51.372, −1.364)) shown in Fig. 1.[35,36] The cut slope was excavated in July 1997, and is 8 m deep and 28 m long. Piezometers were installed in October 2002, with field data available from 2003 to 2008 by Smethurst et al.[37] The slope is mostly uniformly covered by grass and shrubs (see also Fig. 1), with a reported maximum root depth of 800 mm.

The stratigraphy of the site was established from British Geological Survey (borehole id SU46SE120). It comprises of 3 m of weathered London Clay (WLC), 46 m of Intact London Clay (ILC) and 23.5 m of Lambeth Group Clay (LGC - formerly known as Reading beds). The bottom boundary coincided with the Upper Chalk.[38]

2.2. Ecohydrological model

The Tethys-Chloris ecohydrological model (T&C), used in the ecohydrological analysis, is a mechanistic physics-based model that resolves the coupled water, energy and carbon budgets at the soil surface.

Table 1
Hydraulic conductivity of the soil layers.

Soil layer	Weathered LC	Intact LC	Lambeth Group Clay
Hydraulic conductivity (k_{sat}) [m/day]	3.715E−3	3.715E−4	3.715E−4

Table 2
Van-Genuchten SWRC parameters.

Parameter	m [-]	n [-]	α [1/m]	S_{res} [-]	S_{sat} [-]
value	1/3	1.5	0.15	0	1

Water and carbon dynamics (i.e., plant growth) are coupled through well-established biology driven plant physiological responses to the environment and soil water availability. The water and carbon mass balance as well as the surface energy budget are solved in a coupled manner. This coupling leads to a dynamic temporal evolution of vegetation response to weather forcing, which subsequently affects the soil-atmosphere interaction. Ecohydrological dynamics are solved at the hourly timescale using local meteorological forcing. Important components of the hydrological processes such as water inflow, actual transpiration, actual evaporation from ground and snow, interception, run off, surface and sub-surface water fluxes are modelled mimicking the inter-coupled vegetation-hydrology system. A significant part of the actual evapotranspiration is through plant transpiration[39], which T&C resolves as a function of plant structure (particularly of leaf area index) and the response of plant stomata to environmental factors, including atmospheric CO_2 concentration, light availability, temperature and vapor pressure deficit.[40,41] In T&C, ET fluxes are computed by using a big leaf approximation (i.e., neglecting complex 3D radiation effects within complex plant structures), where plant canopies are split just into sun exposed and shaded sections. ET fluxes follow a resistance analogue, where the resistance for vapor fluxes consider plant stomata, soil, and aerodynamic resistance. The model can capture and calculate the saturated and unsaturated soil water flow dynamics. Water movement in the version used in this study is simulated by solving the 1D Richard's equation[42] for variably saturated flow using a finite volume approach discretisation.[32,43–45]

A column of soil with the stratigraphy described in Section 2.1 was considered in the T&C simulations. The plant composition was considered as 70 % shrubs and 30 % grass following visual inspection of the site. The root zone depth was 800 mm and 150 mm respectively for grass and shrubs.[46] The hydraulic conductivities of different soil layers are presented in Table 1 and are in accordance with Smethurst et al.[37] A Van-Genuchten Soil Water Retention Curve (SWRC) [47] was used for the weathered LC, and was derived from interpreted field measurements of suction and water content made by Smethurst et al.[37] The model parameters used are shown in Table 2.

Hydraulic conductivity in the Soil-Plant-Atmosphere continuum comprises of multiple elements, including the hydraulic conductivity at the soil and soil root interface, and the conductivity of sapwood and leaves during plant water ascent.[48] Whilst models that consider the full soil-plant hydraulic complexity exist[40], here a simplified version was used to simulate plant hydraulic limitations to evapotranspiration. Specifically stomatal conductance was reduced from their potential value, according to the Leuning model[49] based on a reduction factor that depends on the root profile averaged soil water potential.[50] Intact London Clay and Lambeth Group Clay were assumed to remain fully saturated due to their high air entry value of suction.[17]

To allow an initialization period, the model was run from January 1990 till the end of the monitoring period 2008. Net inflow/outflow flux was calculated from T&C considering actual evaporation from the ground surface, actual plant transpiration and inflow of water at the soil surface which already accounted for losses due to canopy interception,

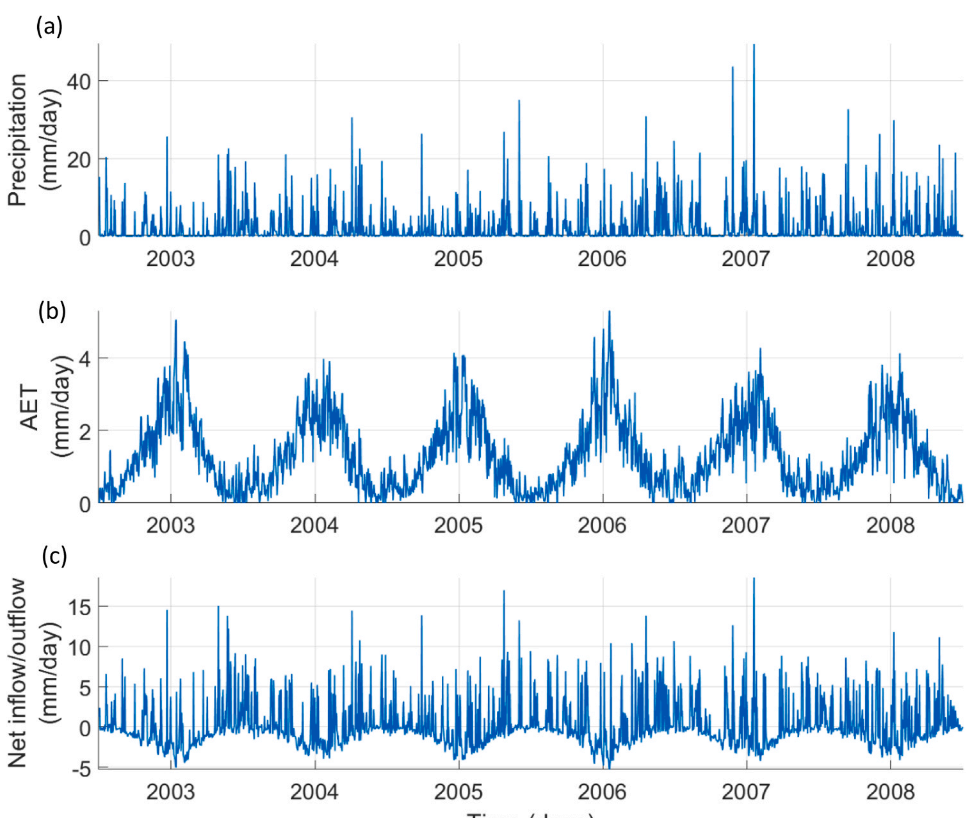

Fig. 2. (a) Precipitation, (b) actual evapotranspiration, and (c) net inflow/outflow boundary condition for the years 2003 till 2008 at the daily scale.

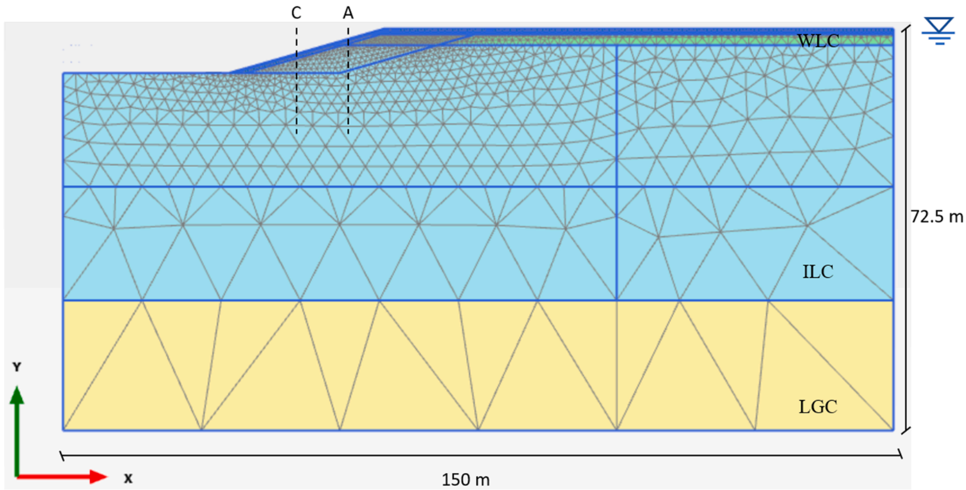

Fig. 3. Cut slope located in Newbury modelled in PLAXIS 2D and its meshing after excavation.

Table 3
Mechanical properties of material for the geotechnical model.

User Defined Soil Model (UDSM) Parameters	User Defined Soil Model (UDSM) Parameters Name	Values
G_{ref} [kN/m^2]	Reference shear modulus	955
K_{ref} [kN/m^2]	Reference bulk modulus	1665
p_{ref} [kN/m^2]	Reference pressure	1
m_G [−]	Nonlinearity of stress-dependency of shear modulus	0.7
m_K [−]	Nonlinearity of stress-dependency of bulk modulus	0.7
a_0 [−]	Basic degradation parameter for $G_{\tan}$	0.181E−3
b[−]	Nonlinearity of degradation of $G_{\tan}$	1.3
$RG_{\min}$ [−]	Normalized degradation limit for $G_{\tan}$	0.05
$G_{\min}$ [kN/m^2]	Minimum shear stress	2000
r_0 [−]	Basic degradation parameter for $K_{\tan}$	0.3E−3
s[−]	Nonlinearity of degradation of $K_{\tan}$	1.1
$RK_{\min}$ [−]	Normalized degradation limit for $K_{\tan}$	0.079
$K_{\min}$ [kN/m^2]	Minimum bulk stiffness	3000
φ [°]	Angle of shearing resistance	23
c[kN/m^2]	Cohesion	7
ψ [°]	Dilatancy angle	0
$G_{\tan}$ [kN/m^2]	Shear stiffness	Ref. 54
$K_{\tan}$ [kN/m^2]	Bulk stiffness	Ref. 54

actual evaporation from intercepted water and snow sublimation.[51] Fig. 2 shows the precipitation and actual evapotranspiration rates calculated from T&C, and the net inflow/outflow rate which was applied as a boundary condition at the soil surface in the geotechnical model. In Fig. 2(c), positive rates correspond to a net inflow, i.e. instances where precipitation exceeded actual evapotranspiration, whereas negative values correspond to the opposite scenario of net outflow, with actual evapotranspiration exceeding precipitation.

2.3. Two-Dimensional geotechnical model

The 2D plane-strain model of the Newbury cut slope can be seen in Fig. 3. It was 150 m wide and 72.5 m deep, consisting of the same stratigraphy as before. A Mohr-Coulomb failure criterion with isotropic small strain stiffness was used for all soil layers.[52] This was implemented into PLAXIS as a User Defined Soil Model (UDSM).[53,54] The mechanical properties of the soil are presented in Table 3 and were derived from the data used previously by O'Brien[14] and Tsiampousi et. al. (2017).[14,19]

This model was selected to simulate the mechanical constitutive behaviour of London clay, despite the fact that it was not developed specifically for unsaturated soils, for its stress- and strain-level dependent nonlinear elastic stiffness. Additionally, as London clay, which is a highly over consolidated clay (its over consolidation ratio can exceed 6–7), was further subjected to unloading in this boundary value problem, wetting-induced collapse, a key feature of unsaturated soil behaviour, was irrelevant. Instead, what was of critical importance in the analysis was the soil shear strength, which is highly overpredicted on the dry side of critical state by unsaturated soil models such as the Barcelona Basic Model[55], as demonstrated by Tsiampousi et al.[56].

Due to lack of comprehensive experimental data that would help quantify the mechanical contribution of the roots for the vegetation covers considered, the conservative assumption was made to ignore it altogether and focus on the hydraulic reinforcement that roots provide by extracting water and increasing suctions. Direct comparisons between different likely vegetation covers are thus possible.

The same hydraulic properties as above were used. Further to the previous models, a User Defined Flow Model (UDFM) that incorporates non-linear anisotropic variation of permeability with mean effective stress was used for all soil layers, so that the vertical hydraulic conductivity value decreased from its initial value with increasing mean effective stress.[57] This was done by using Eq. 1.

$$k_v = k_{y,ref} e^{ap'} \tag{1}$$

where $k_{y,ref}$ is the reference permeability along the y direction, k_v is the current vertical permeability, p' is the mean effective stress and a is a fitting parameter. a was taken as 0.007 in accordance with Kovacevic et al.[58] Due to the fact that water movement within the slope has a 2D nature, the ratio between the horizontal and vertical permeabilities needed to be defined. A ratio of 10, as proposed by Wongsaroj et al.[59] was chosen here.

To initialize the stresses a unit weight of 20 kN/m^3 was specified for all soil layers, above and below the ground water table which was assumed to be initially at 1 m of depth.[60] The initial pore water pressure distribution was assumed to be hydrostatic. The coefficient of earth pressure at rest (K_0) was 1.2, 1.5 and 1.0 for WLC, LC and LGC, respectively, i.e. typical of the over consolidation that London and Lambeth group clays have experienced in their geological past.

The excavation of the 8 m deep cutting was simulated first over three undrained phases of the analysis. It was followed by a fully coupled flow-deformation analysis, for the years 1997, when the slope was excavated, till 2008, i.e., covering the years for which monitoring data are available (2003–2008), as well as the years before, during which some dissipation of excess PWP generated during the excavation is expected to have taken

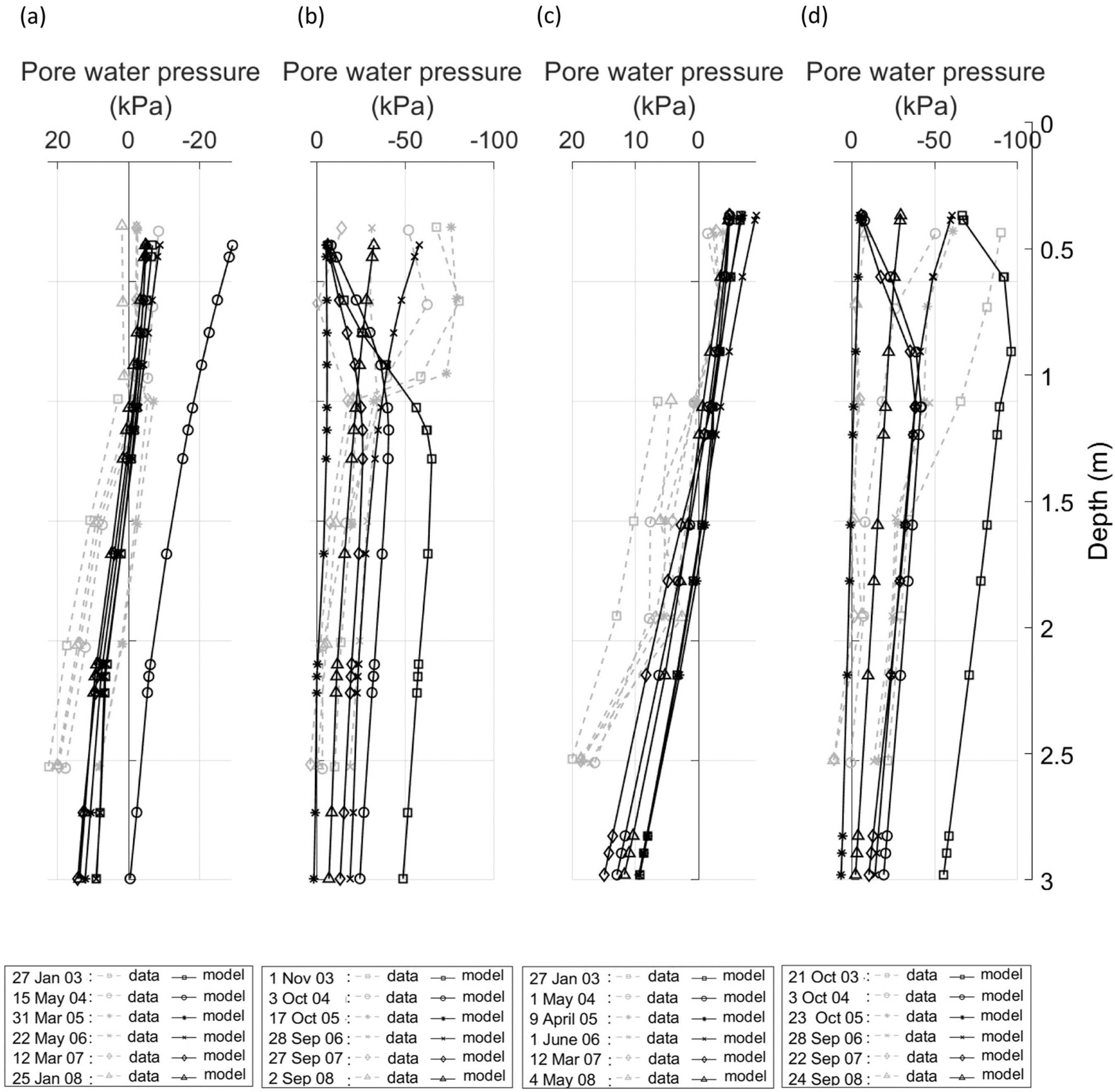

Fig. 4. Comparison of computed and measured PWP variations with depth: (a) winter and (b) summer months for location A, and (c) winter and (d) summer months for location C (suction is shown as negative).

place.

During the coupled part of the analysis, on the ground surface at the slope and the crest (not at the bottom of the cutting where the highway runs), which were uniformly covered with grass and shrubs, the net inflow/outflow rates calculated from T&C were applied. The infiltration boundary condition available in PLAXIS 2D was used to this effect and applied at the soil surface. This is essentially a dual boundary condition that can automatically switch from user defined pore pressure heads to an inflow/outflow water condition with user defined rates. To reduce the computational cost of the geotechnical analysis, the hourly rates calculated from the T&C output were aggregated to the daily scale. The maximum allowable head was set to −0.5 m (5 kPa of suction) in order to maintain a realistic water table. The minimum allowable head was set to −100 m (i.e., a suction of 1000 kPa).[61]

The axis of symmetry and the right-hand side vertical boundaries were impermeable, whereas water could seep freely through the bottom boundary at the interface with the permeable chalk. The PWPs within the soil were allowed to change seasonally in accordance with the applied infiltration boundary condition.

The factor of safety (FoS) was calculated in selected time instances through secondary drained analyses, initiating from the main analysis and applying the strength reduction technique explained by Potts and Zdravkovic (2012) and Tsiampousi et al. (2013).[62,63] The FoS applied to the angle of shearing resistance was progressively increased from 1 as shown in Eq. 2, until slope failure was obtained:

$$\tan\varphi^{F_s} = \frac{\tan\varphi'}{F_s} \tag{2}$$

where F_s is the FoS and φ' and φ^{F_s} are the actual and factored shearing

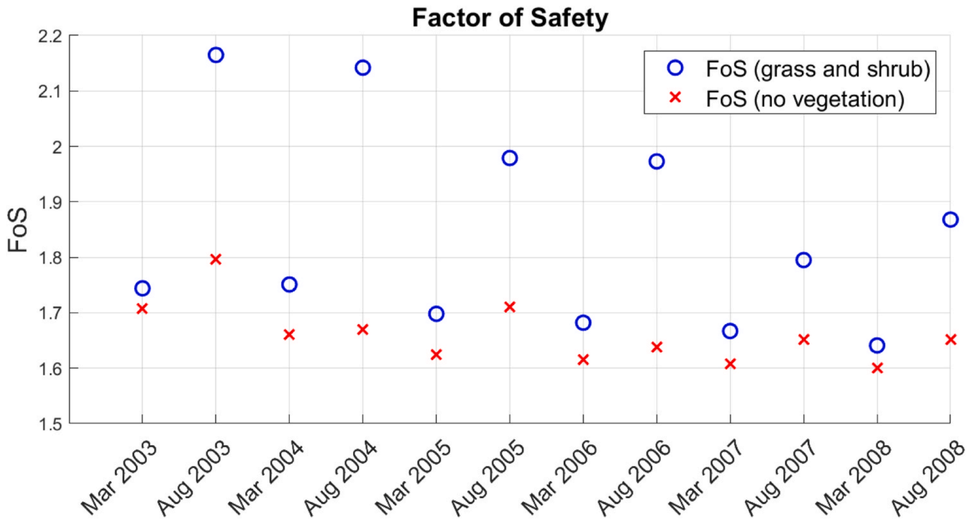

Fig. 5. FoS variation with time for when it is covered with grass and shrub and when it is bare.

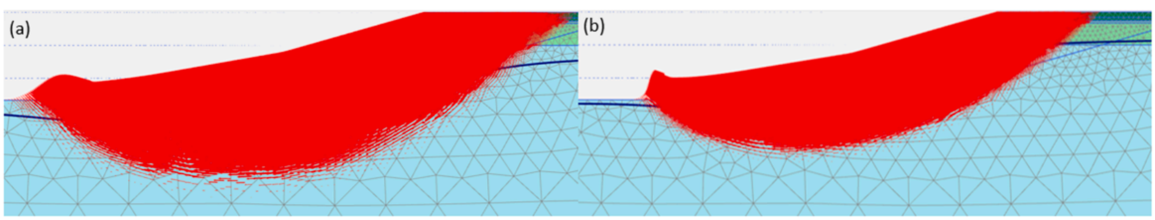

Fig. 6. Failure surface in August 2003 for (a) cut slope covered with vegetation and (b) bare cut slope (The existence of a failure mechanism is demonstrated by the relative (not the actual) magnitude of the vectors).

resistance angle, respectively.

2.4. Model validation

Field data of PWPs with depth were available at different times at the two locations shown in Fig. 3 as A and C, 24 and 12 m from the toe of the slope, respectively. Fig. 4 shows the comparison between field and numerical data, for the first 3 m from the ground surface. The solid lines correspond to the analysis results and the dotted lines to the field measurements from Smethurst et al.[37] The computed and measured PWP variations with depth agree in terms of order of magnitude, range and trends. The observed discrepancies can be attributed to the fact that the PWP measured in the field and calculated in the analysis have resulted from coupled transient phenomena, meaning that both of them represent a snapshot in time. Given the nonlinearity of the boundary conditions applied and of the soil hydraulic properties, the simplifications that inevitably need to be made in the analysis (e.g. soil homogeneity), the limitations of field instrumentation (e.g. time required for devices to reach equilibrium) and the incremental nature of time in the analysis, the differences observed are not surprising. Furthermore, coupled interactions with the mechanical model (where void ratio changes and plasticity also generate water flow and PWP changes) further complicate the mechanisms behind PWP predictions. Therefore, capturing the general trends in suction variation with depth and time provides validation for several features in the analyses beyond the boundary conditions and the hydraulic parameters considered. Despite the obvious challenges, the numerical model captured the seasonal trends and magnitudes of PWP satisfactorily.

The variation of FoS with time is shown in Fig. 5 in blue circles. Larger FoS was consistently obtained for August in comparison to March of each year. A trend of seasonally varying but overall dropping FoS was observed, which can be attributed to the combination of soil-plant-atmosphere interaction and the dissipation of tensile excess PWPs that were generated during the undrained excavation.

The FoS for a bare slope are also shown in Fig. 5, in red. As expected, the lack of vegetation in this analysis led to smaller FoS, the differences with the vegetated slope being especially pronounced during summer months when actual transpiration rates were high.[19,20,64] The corresponding slip surfaces for August 2003 for the vegetated and bare slopes are shown in Fig. 6. The slip surface for the vegetated slope was deeper, due to the added effect of actual transpiration, included in the surface boundary condition. The small seasonal variations of FoS in the bare slope were due to actual evaporation. The general reduction of FoS with time, similar to the vegetated slope, can again be attributed to the dissipation of tensile excess PWPs that were generated during the undrained excavation.

Dissipation of excess PWPs and swelling, and interaction of the slope with the atmosphere through SPAI are two processes that happen simultaneously but are driven by different mechanisms. Swelling happens because of differences in head between the short-term and the steady-state and it would happen independently of any interaction with the atmosphere, i.e. even in the absence of any SPAI. SPAI is driven by the applied inflow/outflow, and therefore, by actual evaporation and actual transpiration, and would carry on happening after all excess PWPs have dissipated.

Similar observations for a grass covered cut slope were made by Tsiampousi et al. (2017).[19]

3. Future slope behaviour

3.1. Climate projections

The effect of climate change on the stability and serviceability of the cut slope was investigated to identify correlations between projected

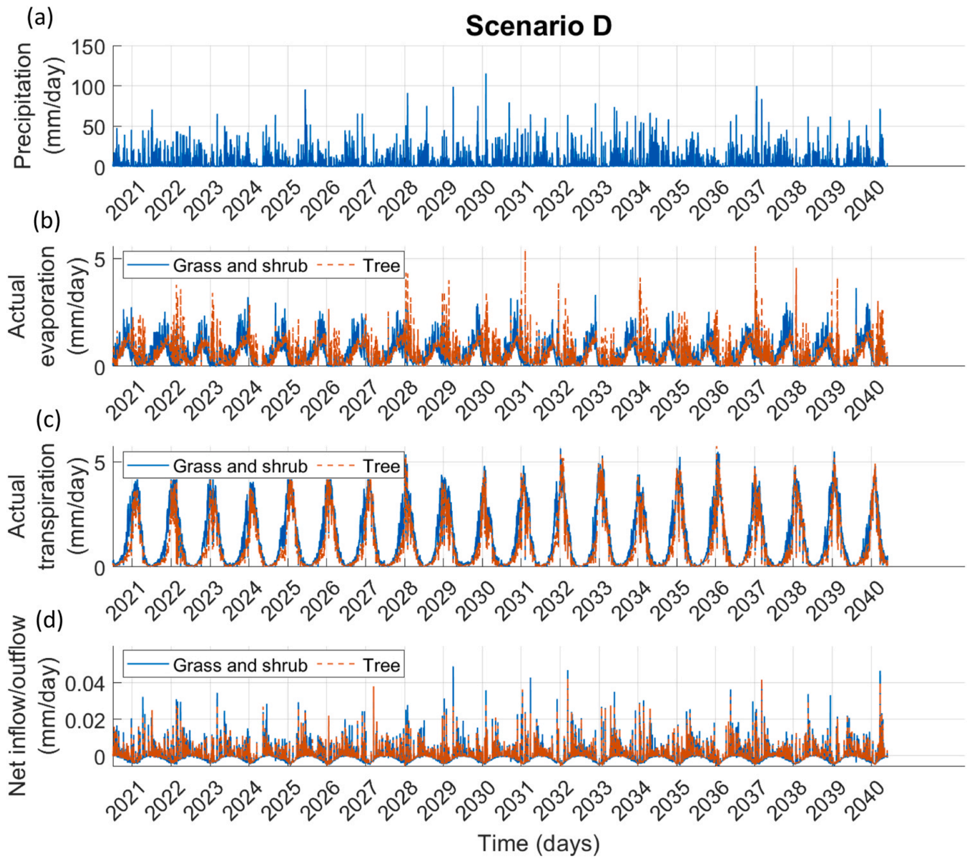

Fig. 7. (a) Precipitation, (b) actual evaporation, (c) actual transpiration, and (d) net inflow/outflow BC for scenario D (driest scenario) against time.

rainfall and actual evapotranspiration of different vegetation covers, and slope behaviour. UKCP18, which is the most updated assessment of how UK's climate will change over the 21st century, was considered. UKCP18 uses probabilistic projections over land and generates a set of high-resolution future climate projections.[65]

UKCP18 projections are available for different Representative Concentration Pathways (RCP). For the purpose of this paper, RCP8.5 was used, which is the worst-case scenario pathway where no climate mitigation is employed. [66–69] UKCP18 has produced 12 ensemble members for the RCP8.5 scenario. After examining these scenarios with standard grass and shrub cover, the two most extreme cases, i.e., the driest and the wettest, were chosen from the calculated net precipitation and actual evapotranspiration, and are referred to here as D and W, respectively. The climatic data from these two scenarios were used in T&C for two different vegetation covers: A) 70 % / 30 % vegetation cover of evergreen grass and shrubs, and B) a mixture of tree cover with a root zone depth of 1000 mm (calibrated to resemble the UK weather conditions and a cover of silver birch and common hazel, i.e. a deciduous and an evergreen type, respectively).

Fig. 7(a) shows the precipitation and Fig. 7(b) shows the actual evaporation rates for the driest scenario, D. Overall trees gave the highest actual evaporation rates, justified by their larger canopies intercepting more rainfall water than grass and shrubs, and thus accommodating more water to be evaporated directly from their leaves. Actual transpiration rates over the years were slightly higher for grass and shrubs than for trees (see Fig. 7(c)), in accordance with the fact that tree cover is comprised of both a deciduous and evergreen type, but grass and shrubs are both evergreens. When combining the above T&C output to calculate net inflow/outflow (Fig. 7(d)) a complicated picture arose, with instances of either grass and shrubs or trees yielding the highest net inflow (i.e. positive net rate), but with trees almost consistently demonstrating smaller net outflow (i.e. negative net rate). The complexity is due to the multiple factors affecting actual plant transpiration, including the responses of plant stomata to raising CO_2 and atmospheric dryness (e.g., vapor pressure deficit), stomata responses to soil water deficits, as well as limitation of plant growth due to plant water stress.

Fig. 8 shows precipitation, actual evaporation, actual transpiration, and net inflow/outflow for the wettest scenario, W. The same trends as in scenario D can be observed. When comparing Fig. 7 and Fig. 8, as expected, precipitation was overall higher for the wettest scenario, W, meaning that more water was available for evaporation, leading to higher actual evaporation rates for scenario W than for scenario D. Since the vegetation covers and water demand were the same, actual transpiration rates for both scenarios were similar, resulting in higher actual evapotranspiration rates for scenario W. Overall higher net inflow/outflow rates were obtained for scenario W.

3.2. Geotechnical analysis results

The combinations of two climate scenarios and two vegetation covers were considered in four 2D PLAXIS analyses, where the net inflow/outflow shown in Fig. 7(d) and 8 (d) was applied, using the infiltration boundary condition as explained earlier. These four analyses were all initiated from the end of the analysis described in Section 2.3 allowing an initialisation period of 11.5 years with a uniform grass and shrub cover, before the four climate projection scenarios were applied in the subsequent 20 years.

Fig. 9(a) shows the annual cumulative net inflow/outflow rate and Fig. 9(b) shows the FoS calculated in the numerical analysis at selected time instances for the driest and wettest scenarios, D and W, respectively, for the grass and shrub vegetation cover, for the years 2021, 2025, 2030, 2035 and 2040. In both scenarios the reducing trend of FoS with time that was seen in Fig. 5 was reversed, as dissipation of excess

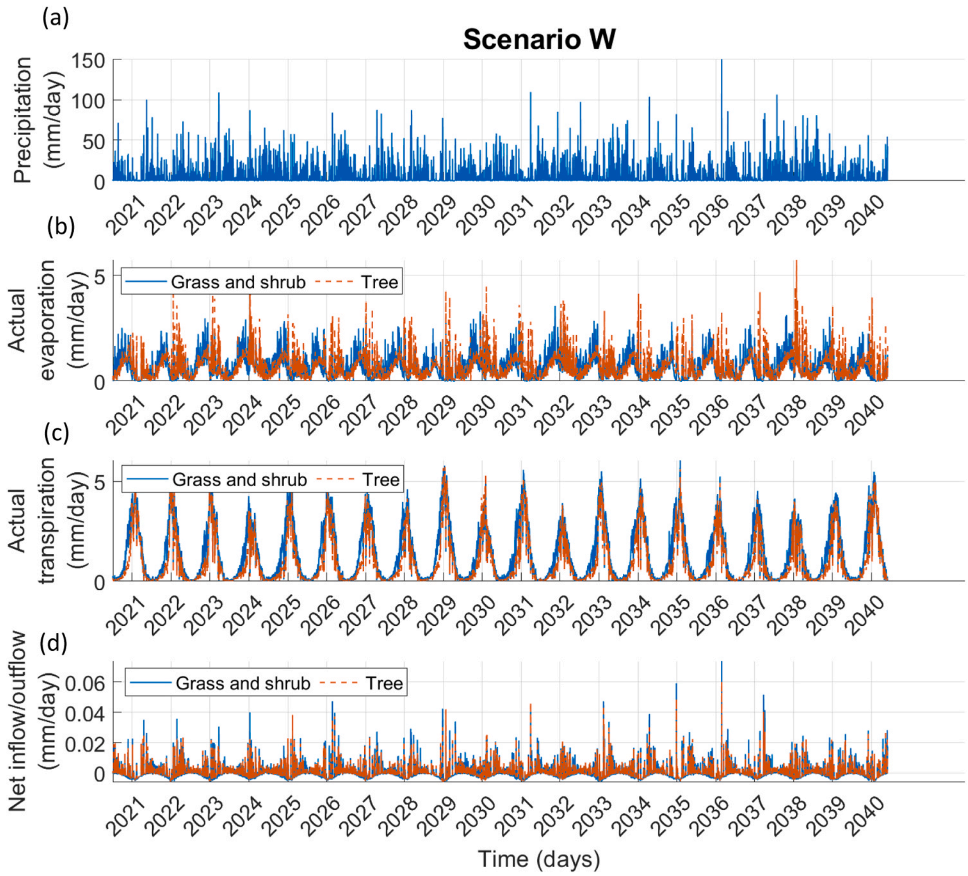

Fig. 8. (a) Precipitation, (b) actual evaporation, (c) actual transpiration, and (d) net inflow/outflow BC for scenario W (wettest scenario) against time.

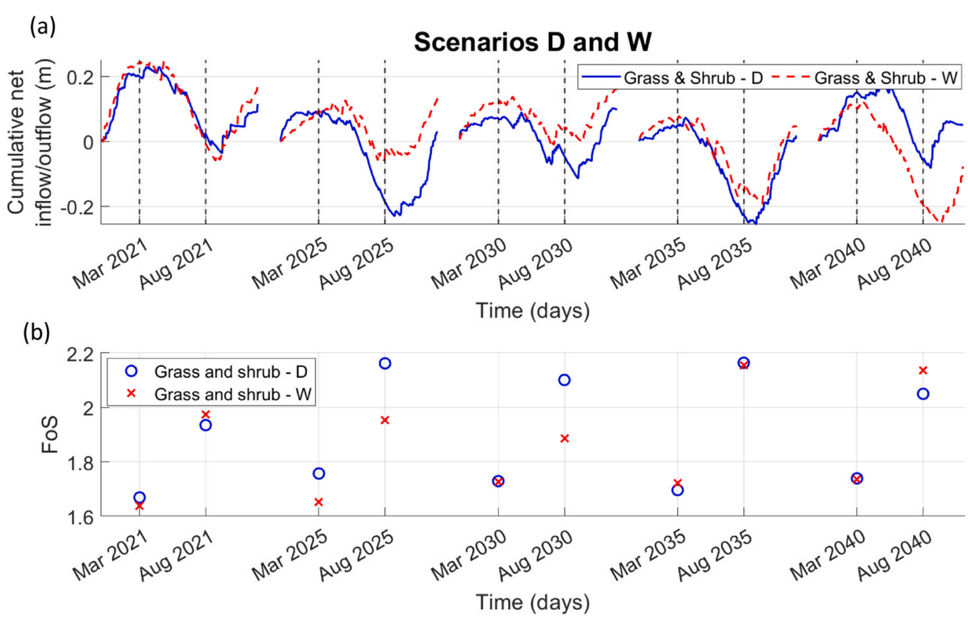

Fig. 9. (a) Annual cumulative net inflow/outflow, and (b) FoS variation with time for climate scenarios D and W for grass and shrub vegetation cover.

PWPs was nearly completed. The August-March trend that was discussed in relation to Fig. 5 was maintained.

Comparing the results for the two scenarios, intuitively, it would perhaps be expected that larger inflow rates would lead to higher PWP and subsequently lower FoS, as it can be seen in March and August 2021. Although this was true for some of the time instances examined, it was not universally applicable. For example, in March 2030, even though the two scenarios had different inflow rates, the FoS were very similar.

From Fig. 10, it can be seen that the two analyses yielded very similar suctions in March 2030, which were quite low in magnitude in accordance with the time of the year. Inflow in the two analyses was limited by soil permeability and the soil-water retention curve, which, at very

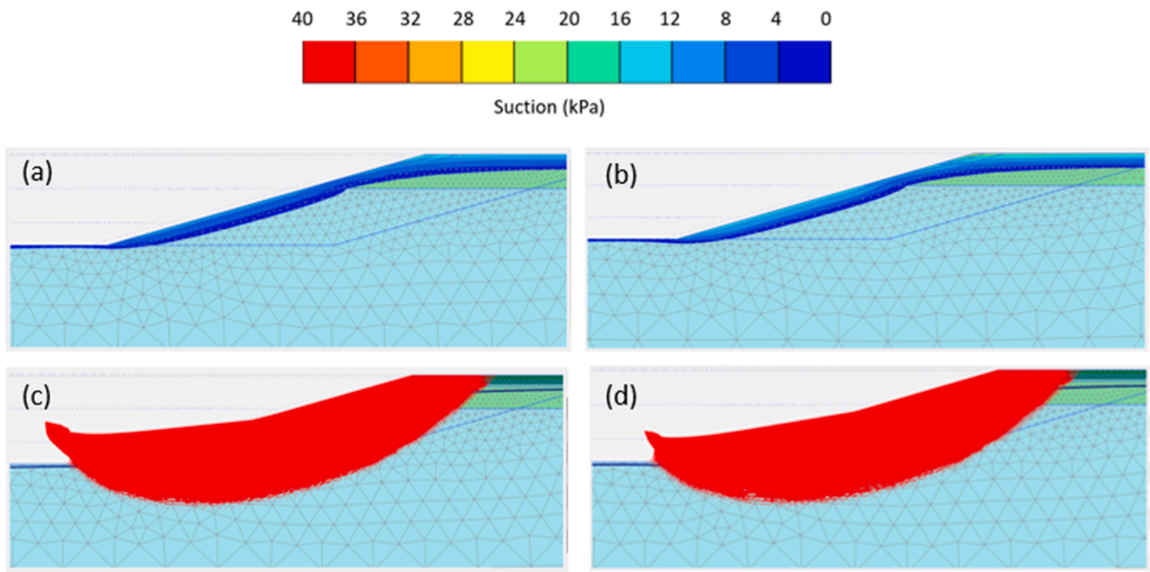

Fig. 10. (a) Contours of suction for grass and shrub for driest scenario D and (b) wettest scenario W, (c) vectors of incremental displacement at failure for grass and shrub cover for driest scenario D and (d) wettest scenario W in March 2030.

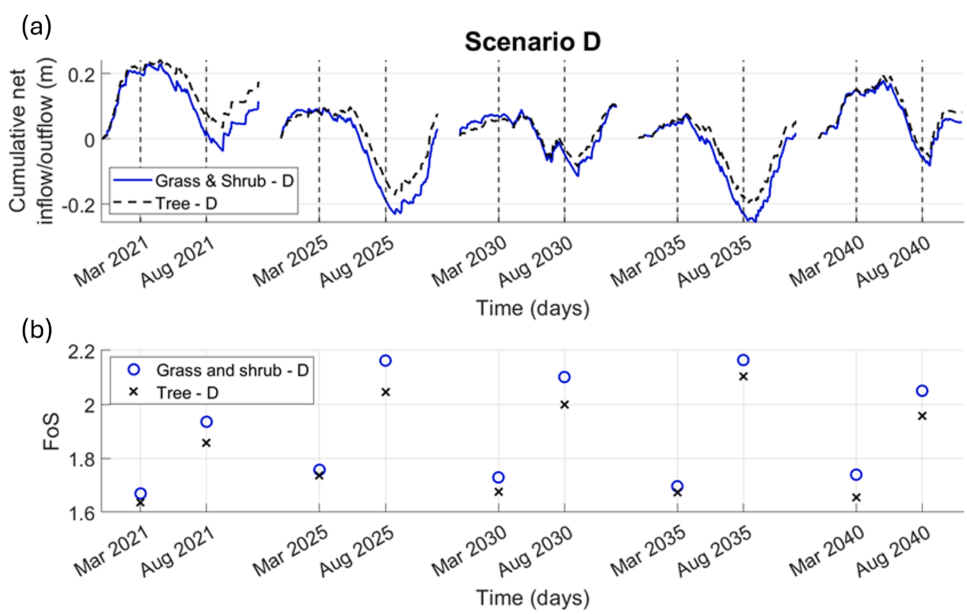

Fig. 11. (a) Annual cumulative net inflow/outflow, and (b) FoS variation with time for climate scenario D for two different vegetation covers.

low suctions, were nearing their saturation values and were therefore similar in the two analyses. Consequently, the operational inflow rates were similar, justifying the similarities in suction values and by extension in FoS and in failure mechanisms (also shown in Fig. 10). Similar points can be raised for the remaining times instances, demonstrating that, even for a given vegetation, reliance on climate data alone to explain FoS is not adequate.

Results for different vegetation covers but the same climate projection scenarios are given in Figs. 11 to 16. Fig. 11 (a) shows the annual cumulative net inflow/outflow rate and Fig. 11 (b) compares the FoS calculated for scenario D for grass and shrubs, and trees. As explained in relation to Fig. 7, tree cover resulted in lower overall net outflow rates, therefore, it is not surprising that generally smaller FoS were computed when compared with the grass and shrubs cover. Although the FoS trends observed were generally supported by the yearly cumulative net inflow/outflow, there were some exceptions: for example, in March 2040 the cumulative net flow showed little visible difference between the two analyses, whereas distinct FoS values were calculated. The 30, 10, 5 and 2 days cumulative and last day's net flows prior to the FoS calculation are presented in Fig. 12, showing that (with the exception of the 30-day cumulative net inflow) in the days prior to the calculation of FoS, net inflow rates were higher for trees, resulting in slightly lower suctions in the slope (Fig. 13) and therefore a slightly lower FoS.

Further to previous observations, no clear association between annual cumulative net inflow/outflow and FoS could be readily established from the analyses simulating grass and shrubs, and tree covers, for the wettest scenario W (Fig. 14). For example, FoS values in August 2025 were very similar, despite the different cumulative net flows. The similar FoS values cannot be explained by the net outflow rate in the days prior to the calculation of FoS, which were also dissimilar (Fig. 15), however, they can be explained by the computed suction contours, shown in Fig. 16 to be very similar.

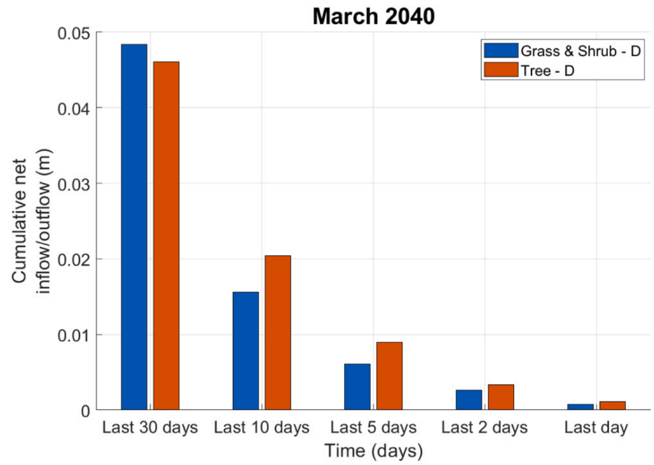

Fig. 12. Cumulative net inflow/outflow rate for the last 30, 10, 5, and 2 days as well as the last day for both grass and shrub vs trees for the driest scenario D in March 2040.

Fig. 17 presents the vertical displacement, sub-accumulated from the end of excavation, at the bottom of the excavation with distance from the centreline, for various time instances for scenarios D and W, for grass and shrubs cover. The sub-accumulated vertical displacement prior to climate projection is also shown for comparison. In March 2040 (Fig. 17 (a)) larger swelling was predicted for scenario W, although the annual cumulative net inflow rates for scenario D were larger (Fig. 9(a)). The difference in vertical displacements can be attributed to the accumulation of swelling and/or lack of shrinkage in scenario W in previous months and years. In contrast, in August 2040 (Fig. 17 (b)), the

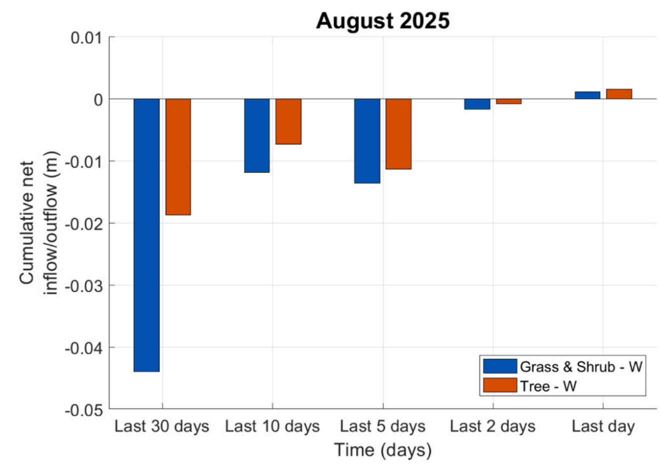

Fig. 15. Cumulative net inflow/outflow rate for the last 30, 10, 5, and 2 days as well as the last day for both grass and shrub vs trees of the wettest scenario W for August 2025.

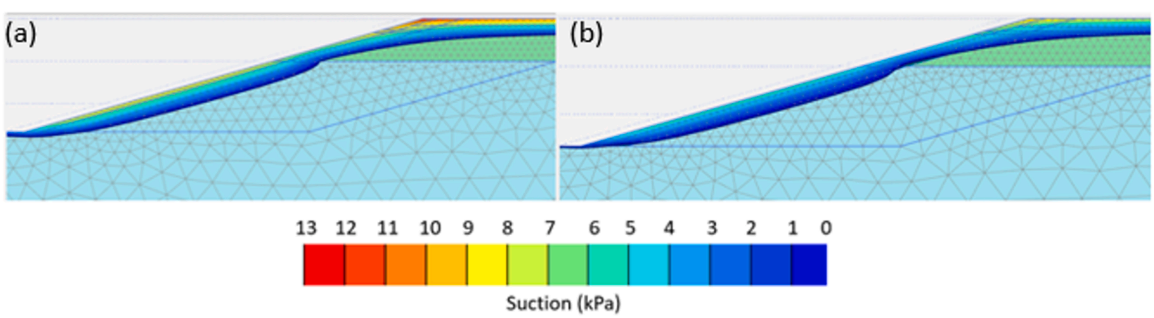

Fig. 13. (a) Contours of suction for grass and shrub and (b) for tree for driest scenario D in March 2040.

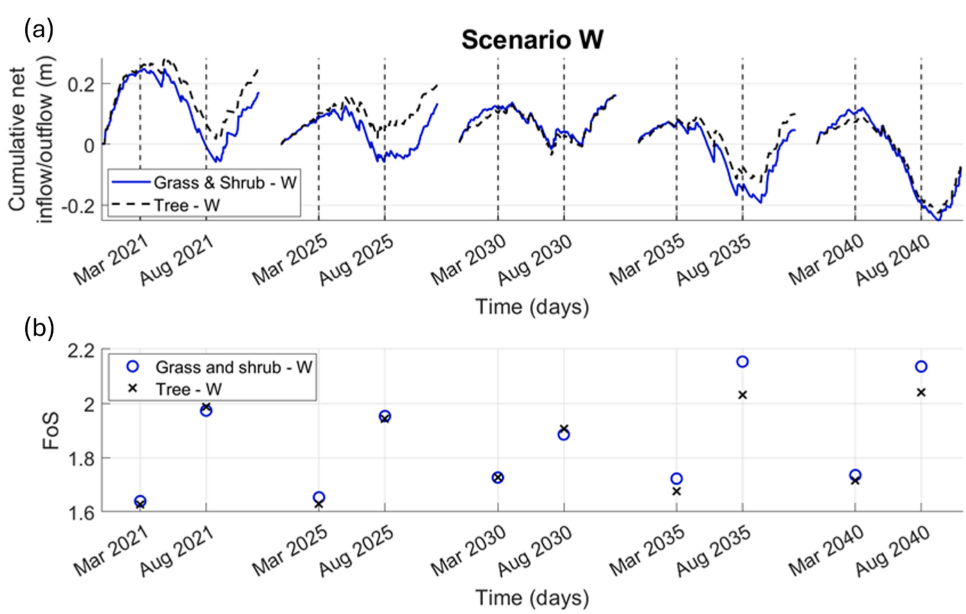

Fig. 14. (a) Annual cumulative net inflow/outflow, and (b) FoS variation with time for climate scenario W for two different vegetation covers.

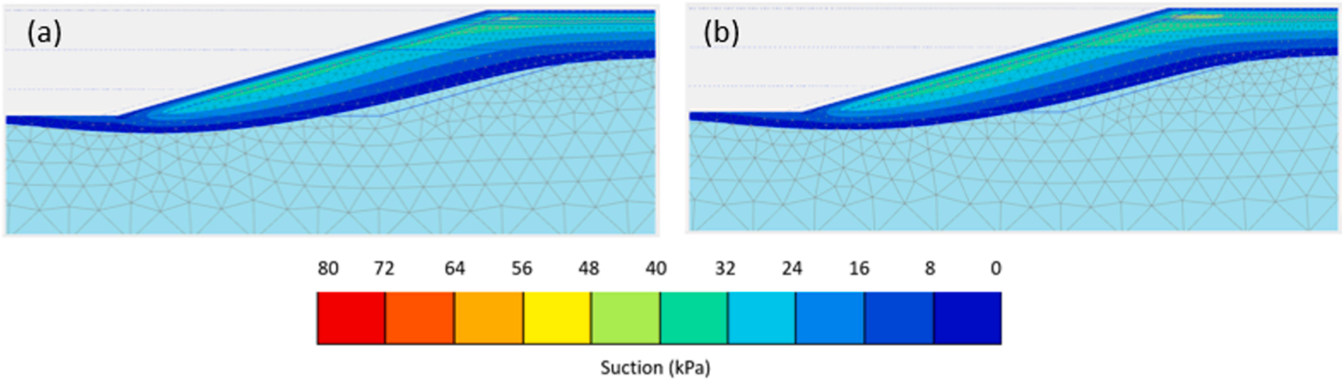

Fig. 16. Contours of suction for the wettest scenario W for (a) grass and shrub and (b) tree vegetation cover in August 2025.

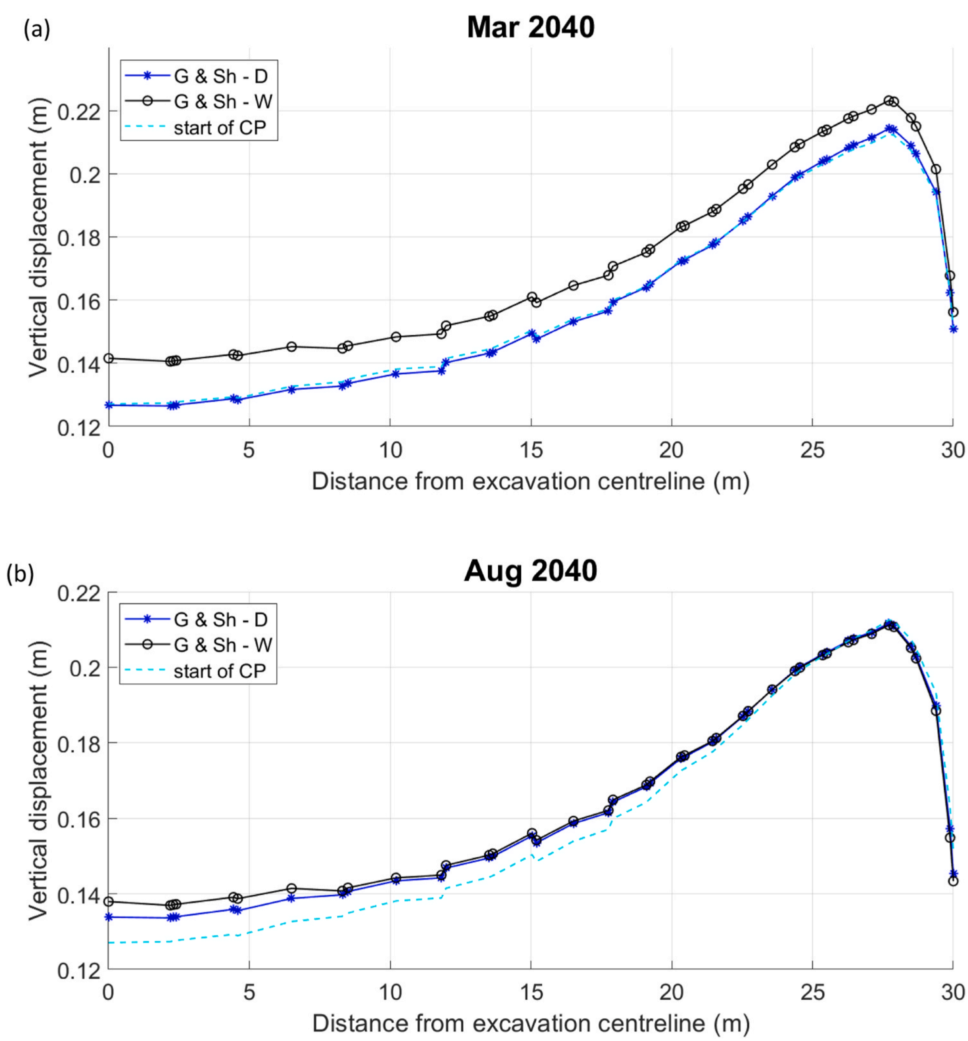

Fig. 17. Vertical displacement at the bottom of the excavation against distance from the excavation center line for climate scenarios D vs W and for grass and shrub vegetation cover and the beginning of the climate projection analysis in, (a) March 2040 and (b) August 2040.

displacements for the two analyses were very similar, despite the differences in annual cumulative flow rates. This was probably coincidental, with scenario D having produced just enough swelling in relation to March 2040 (due to the particularly wet spring and summer) to catch up with scenario W.

Comparing the sub-accumulated vertical displacements predicted for scenario D for grass and shrubs, and for tree covers in March 2040 (Fig. 18), when the annual net inflow/outflow rates were similar in the two analyses (Fig. 12 (a)), swelling was larger for trees. This is in agreement with the overall larger net inflow in the last 10, 5 and 2 days as discussed earlier (Fig. 13).

When considering the wettest scenario (W), the tree cover yielded consistently larger swelling than the grass and shrubs cover in August of years 2025 and 2035 (Fig. 19), in agreement with their annual cumulative values (Fig. 14 (a)). From the displacements for August 2025 in particular, for which contours of suction have been presented in Fig. 15

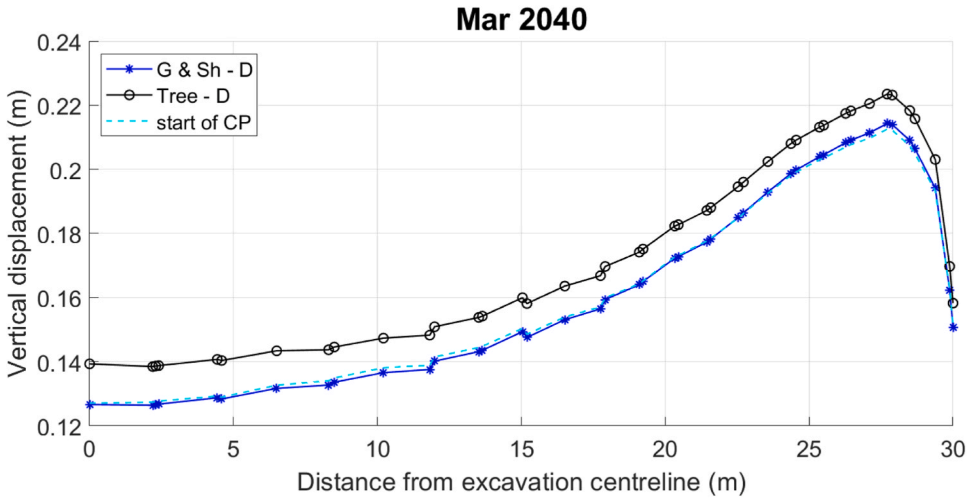

Fig. 18. Vertical displacement at the bottom of the excavation against distance from the excavation center line for climate scenarios D for grass and shrub vs tree and the beginning of the climate projection analysis in March 2040.

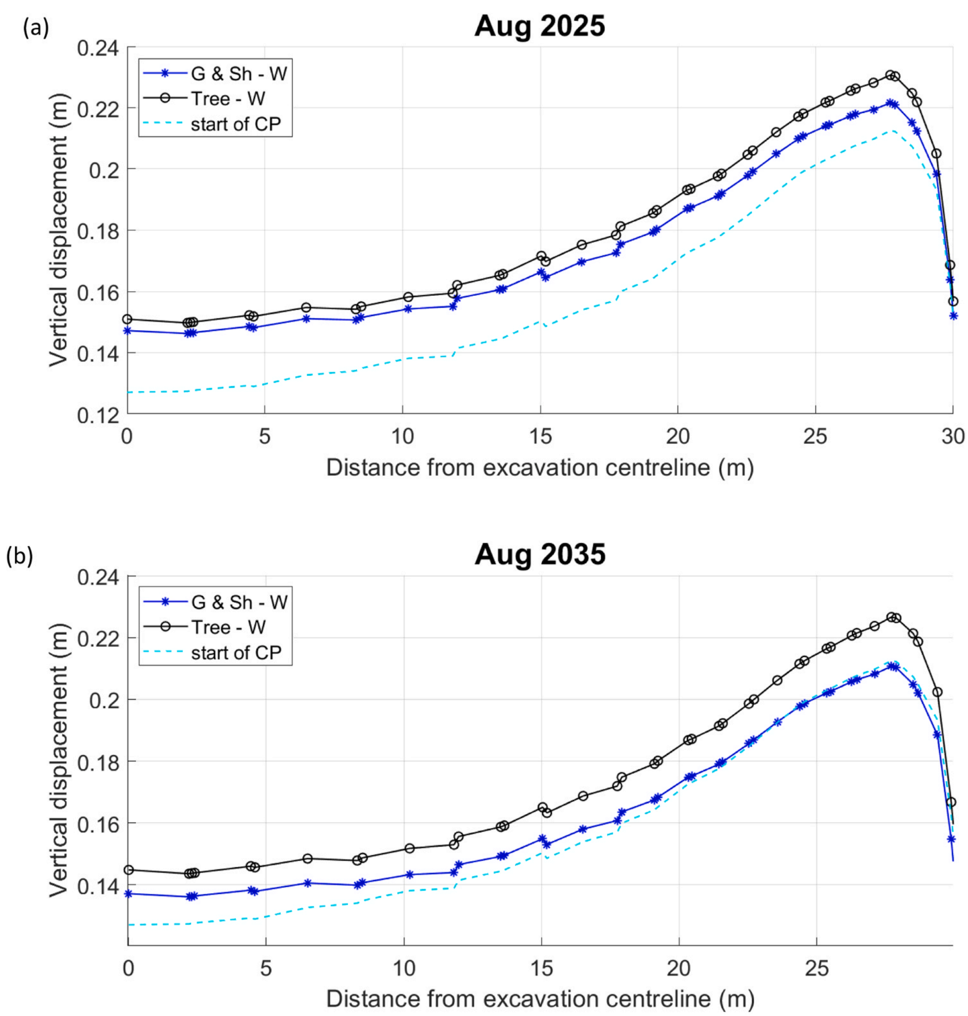

Fig. 19. Vertical displacement at the bottom of the excavation against distance from the excavation center line for climate scenarios W for grass and shrub vs tree and the beginning of the climate projection analysis in (a) August 2025 and (b) August 2035.

to be very similar for the two analyses, it can be deduced that magnitudes of suction cannot be correlated to soil swelling/shrinkage. As volumetric changes result from changes in stress or suction, snapshots of suction contours can provide no information regarding displacements, although they can be related to FoS values.

3.3. Discussion

The results discussed above support the argument that the applied boundary conditions on their own are not capable of giving an accurate description of the likely mechanical response of the slope. Water inflow is limited by the hydraulic soil properties, permeability and water retention, and water extraction is limited by the availability of ground water, meaning that antecedent conditions play a major role on the impact that the applied boundary conditions have on the calculated FoS. It was not possible to identify any clear evidence of potential correlations between the applied boundary conditions and FoS. Different annual cumulative rates produced similar FoS values in same cases and dissimilar in other. Equally, similar annual cumulative rates produced different FoS values in certain cases. In some of these cases, the cumulative net inflow/outflow for the days prior to the FoS calculation could justify the computed FoS, in others not. Where the applied boundary conditions on their own failed to explain the results, suction contours, as expected, did provide adequate justification, as there is a direct link between the value of suction and operational strength in the constitutive model.

There were instances where net inflow/outflow rates accumulating over the days and months prior to the calculation of FoS, rather than the annual cumulative rates, could help explain the values of FoS. Nonetheless, it was not possible to identify clear evidence of correlations between the last 30,10,5, and 2 days cumulative and last day's net inflow/outflow and FoS.

The mechanical reinforcement of the roots was neglected in the analysis to isolate the hydraulic reinforcement. The analysis results indicated that grass and shrubs provide adequate and arguably better hydraulic reinforcement than trees. This was justified by the balance between precipitation, leaf interception, actual evaporation from leaves and actual transpiration for the two different vegetation cover. Again, intuitively, it may be expected that trees would provide better hydraulic reinforcement, but this expectation was not corroborated here. Although trees have deeper roots than the grass and shrub cover, there was not much difference in their actual transpiration rates. Furthermore, actual transpiration was combined with inflow to calculate the net rates that were applied as a surface boundary condition in the analysis. This is a limitation that needs to be addressed in future research, as where the water is extracted from is of significance.

FoS values remained healthy for this well-designed slope under the combined effect of excess tensile pwp dissipation and soil-atmosphere interaction, and under the examined climate projections. There was some incentive in using grass and shrubs in the driest scenario and benefits from grass and shrubs could still be observed in the wettest scenario.

Finally, it was not possible to identify evidence of correlations between the applied boundary conditions and the volumetric behaviour of the slope. For example, cases were discussed where similar net inflow/outflow rates led to dissimilar vertical displacements at the bottom of the slope, even when suction contours were very similar. Although water inflow may be limited by the hydraulic soil properties, swelling may have already accumulated in previous days and months. The applied boundary conditions indirectly trigger volumetric soil changes by inducing suction changes. Although suction changes can be clearly correlated to volume changes through the mechanical soil properties (bulk stiffness and soil compressibility), indirect links between applied boundary conditions and volume changes are probably too complex and dependent on far too many factors to be readily identifiable. The analyses results indicated that serviceability of the examined slope under the examined conditions is unlikely to either deteriorate or improve drastically.

It should be noted that these observations were made based on a statistically small sample, and it is possible that in the future use of recently advanced tools, such as machine learning, to consider larger data samples, may elucidate interactions and links that are not otherwise easily identifiable.

4. Summary and conclusions

This paper discusses the numerical study of the impact of soil-plant-atmosphere interaction, climate change, and vegetation cover on the behaviour of a cut slope located in Newbury, UK, for which measurements of PWP variation with depth were available. Despite employing a specific slope to validate the numerical model, the observations made, and conclusions drawn transcend the specific case study and can provide useful insights into the stability and serviceability of similar clay slopes in the UK and in places around the world with similar climatic conditions.

The hydrological processes were calculated using the ecohydrological model T&C which accounts for the effect of climate and vegetation cover in a realistic manner at the surface of the soil and with depth. T&C output was translated into appropriate boundary conditions to a geotechnical analysis conducted with PLAXIS. Distribution of PWPs against depth at various time instances was compared with available field measurements over a period of six years, validating the model and the applied methodology.

Two different climate projection scenarios, accounting for the wettest and driest futures, were analysed and two different vegetation covers were considered, grass and shrub, and trees, resulting in four additional geotechnical analyses. Despite an annual variation of FoS and differences between the four analyses, FoS values adequately large for slope stability were systematically computed. The swelling at the bottom of the excavation at selected time instances primarily at the end of dry periods indicated no dramatic changes in serviceability.

Although climatic data are the driving force behind seasonal and annual changes in the stability and serviceability of the slope, it was not possible to correlate them directly to FoS and to displacement trends. Despite their undeniable importance and usefulness, they are unlikely to be sufficient on their own to explain and predict slope stability. Although snapshots of suction helped explain the stability of the slope, changes in suction would be needed to explain its serviceability. Therefore, monitoring of suctions and suction changes, as well as of displacements, cannot and should not be replaced by monitoring of climatic conditions alone. This important conclusion can only be drawn with confidence thanks to the advanced ecohydrological modelling of the vegetation cover, which resulted in reliable climatic conditions used in the geotechnical analysis.

CRediT authorship contribution statement

Athanasios Paschalis: Writing – review & editing, Supervision, Software, Methodology, Funding acquisition, Conceptualization. **Aikaterini Tsiampousi:** Writing – review & editing, Supervision, Software, Methodology, Funding acquisition, Conceptualization. **Maryam Sadat Maddah Sadatieh:** Writing – original draft, Visualization, Methodology, Funding acquisition, Formal analysis, Conceptualization.

Declaration of Competing Interest

The authors declare that they have no known competing financial interests or personal relationships that could have appeared to influence the work reported in this paper.

Acknowledgement

This work was supported by the Natural Environment Research Council [grant number: NE/S007415/1]; the Skempton Scholarship from Imperial College London; and CASE partner Geotechnical Observations Limited. The Tethys – Chloris (T&C) model code is available at the following link: https://codeocean.com/capsule/0294088/tree/v3. doi.org/10.24433/CO.0905087.v3

Appendix A. Supporting information

Supplementary data associated with this article can be found in the online version at doi:10.1016/j.gete.2025.100697.

Data availability

Data will be made available on request.

References

1. Perry J, Pedley M, Reid M. *Infrastructure embankments - condition appraisal and remedial treatment. CIRIA Report C550.* Published online; 2001.
2. Perry J, Pedley M, Reid M. *Infrastructure cuttings - condition appraisal and remedial treatment. CIRIA Report C591.* Published online; 2003.
3. Office of rail and road. *Annual Efficiency and Finance Assessment of Network Rail 2021-22.*; 2022.
4. Kilsby C, Glendinning S, Hughes PN, et al. *ClimChange Impacts LongTerm Perform slopes.* 2009;2:59–66. https://doi.org/10.1680/ensu.2009.162.
5. Kandalai S, John NJ, Patel A. Effects of climate change on geotechnical infrastructures — state of the art. *Environ Sci Pollut Res.* 2023;30(7):16878–16904. https://doi.org/10.1007/s11356-022-24788-7.
6. Vardon PJ. Climatic influence on geotechnical infrastructure: a review. *Environ Geotech.* 2015;2(3):166–174. https://doi.org/10.1680/envgeo.13.00055.
7. Lowe J.A., Bernie D., Bett P., et al. *UKCP18 Science Overview Report.*; 2018. ⟨www.metoffice.gov.ukwww.metoffice.gov.uk⟩.
8. *UK Climate Projections : Headline Findings.*; 2021. Accessed November 6, 2024. ⟨www.metoffice.gov.uk⟩.
9. Moustakis Y, Papalexiou SM, Onof CJ, Paschalis A. Seasonality, intensity, and duration of rainfall extremes change in a warmer climate. *Earths Future.* 2021;9(3). https://doi.org/10.1029/2020EF001824.
10. Dehn M., Bü Rger B.G., Buma J., Gasparetto P. *Impact of Climate Change on Slope Stability Using Expanded Downscaling.* Vol 55.; 2000. ⟨www.elsevier.nl/locate/enggeo⟩.
11. Alonso EE, Gens A, Delahaye CH. Influence of rainfall on the deformation and stability of a slope in overconsolidated clays: a case study. *Hydrogeol J.* 2003;11(1):174–192. https://doi.org/10.1007/s10040-002-0245-1.
12. Jamalinia E, Tehrani FS, Steele-Dunne SC, Vardon PJ. A data-driven surrogate approach for the temporal stability forecasting of vegetation covered dikes. *Water (Switz).* 2021;13(1). https://doi.org/10.3390/w13010107.
13. Tang AM, Cui YJ, Trinh VN, Szerman Y, Marchadier G. Analysis of the railway heave induced by soil swelling at a site in Southern France. *Eng Geol.* 2009;106(1-2):68–77. https://doi.org/10.1016/j.enggeo.2009.03.002.
14. O'Brien AS, Ellis EA, Russell DD. Old railway embankment clay Fill-Laboratory experiments. *Numer Model Field Behav.* 2004.
15. Lees AS, MacDonald GJ, Sheerman-Chase A, Schmidt F. Seasonal slope movements in an old clay fill embankment dam. *Can Geotech J.* 2013;50(5):503–520. https://doi.org/10.1139/cgj-2012-0356.
16. Rouainia M, Davies O, O'brien T, et al. *Numerical modelling of climate effects on slope stability.* Published online; 2009. https://doi.org/10.1680/ensu.2009.162.
17. Tsiampousi A, Day C, Petalas A. Engineering soil barriers to minimise annual shrinkage/swelling in plastic clays. *Geomech Energy Environ.* 2024;38. https://doi.org/10.1016/j.gete.2024.100540.
18. Jamalinia E, Vardon PJ, Steele-Dunne SC. The effect of soil-vegetation-atmosphere interaction on slope stability: a numerical study. *Environ Geotech.* 2019;8(7):430–441. https://doi.org/10.1680/jenge.18.00201.
19. Tsiampousi A, Zdravkovic L, Potts DM. Numerical study of the effect of soil–atmosphere interaction on the stability and serviceability of cut slopes in London clay. *Can Geotech J.* 2017;54(3):405–418. https://doi.org/10.1139/cgj-2016-0319.
20. Tsiampousi A. *A three-dimensional study of vegetation management on cut slopes. Canadian Geotechnical Journal.* Published online; 2024.
21. An N, Hemmati S, Cui Y. Numerical analysis of soil volumetric water content and temperature variations in an embankment due to soil-atmosphere interaction. *Comput Geotech.* 2017;83:40–51. https://doi.org/10.1016/j.compgeo.2016.10.010.
22. Zeng ZJ, Tang CS, Cheng Q, et al. Numerical analysis of environmental influences on evaporation in a cracked soil slope. *Comput Geotech.* 2024;168. https://doi.org/10.1016/j.compgeo.2024.106126.
23. Cheng Y, Huang X, Li C, Shen Z. Field and numerical investigation of soil–atmosphere interaction at Nairobi, Kenya. *Eur J Environ Civ Eng.* 2017;21(11):1326–1340. https://doi.org/10.1080/19648189.2016.1169224.
24. Assadollahi H, Nowamooz H. Long-term analysis of the shrinkage and swelling of clayey soils in a climate change context by numerical modelling and field monitoring. *Comput Geotech.* 2020;127. https://doi.org/10.1016/j.compgeo.2020.103763.
25. Penman H.L. *Natural Evaporation from Open Water, Bare Soil and Grass.* Vol 193.; 1948. ⟨https://about.jstor.org/terms⟩.
26. Thornthwaite C.W. *An Approach toward a Rational Classification of Climate.* Vol 38.; 1948.
27. Feddes R.A. simulation_of_field_water_use_and_crop_yield-wageningen_university_and_research_172222-Feddes.(n.d).
28. Ng CWW, Guo H, Ni J, Zhang Q, Chen Z. Effects of soil–plant-biochar interactions on water retention and slope stability under various rainfall patterns. *Landslides.* 2022;19(6):1379–1390. https://doi.org/10.1007/s10346-022-01874-y.
29. Wilson G.W., Fredlund D.G., Barbour S.L. *The Effect of Soil Suction on Evaporative Fluxes from Soil Surfaces.*; 1997.
30. Albino UR, Portelinha FHM, Futai MM. Numerical simulation of a geotextile soil wall considering soil-atmosphere interaction. *Geosynth Int.* 2020;27(4):394–413. https://doi.org/10.1680/jgein.20.00003.
31. Rouainia M, Helm P, Davies O, Glendinning S. Deterioration of an infrastructure cutting subjected to climate change. *Acta Geotech.* 2020;15(10):2997–3016. https://doi.org/10.1007/s11440-020-00965-1.
32. Fatichi S, Ivanov VY, Caporali E. A mechanistic ecohydrological model to investigate complex interactions in cold and warm water-controlled environments: 1. Theoretical framework and plot-scale analysis. *J Adv Model Earth Syst.* 2012;4(2).
33. Fatichi S. *Tethys-Chloris (T&C) - terrestrial biosphere model – public release October 2021.* Accessed August 15. Published online 2021; 2024. ⟨https://codeocean.com/capsule/0294088/tree/v2⟩.
34. Sequent. PLAXIS 2D (2023.02). Published online 2023.
35. Smethurst J.A., Clarke D., Powrie W. *Seasonal Changes in Pore Water Pressure in a Grass-Covered Cut Slope in London Clay.* Vol 56.; 2006.
36. Grid Reference Finder. Accessed November 6, 2024. ⟨https://www.gridreferencefinder.com/⟩.
37. Smethurst JA, Clarke D, Powrie W. Factors controlling the seasonal variation in soil water content and pore water pressures within a lightly vegetated clay slope. *Geotechnique.* 2012;62(5):429–446. https://doi.org/10.1680/geot.10.P.097.
38. British Geological Survey; 2024. ⟨https://www.bgs.ac.uk/information-hub/borehole-records/⟩. Accessed November 6.
39. Paschalis A, Fatichi S, Pappas C, Or D. Covariation of vegetation and climate constrains present and future T/ET variability. *Environ Res Lett.* 2018;13(10). https://doi.org/10.1088/1748-9326/aae267.
40. Paschalis A, De Kauwe MG, Sabot M, Fatichi S. When do plant hydraulics matter in terrestrial biosphere modelling? *Glob Chang Biol.* 2024;30(1). https://doi.org/10.1111/gcb.17022.
41. Paschalis A, Katul GG, Fatichi S, Palmroth S, Way D. On the variability of the ecosystem response to elevated atmospheric CO2 across spatial and temporal scales at the duke forest FACE experiment. *Agric Meteor.* 2017;232:367–383. https://doi.org/10.1016/j.agrformet.2016.09.003.
42. Richards LA. Capillary conduction of liquids through porous mediums. *J Appl Phys.* 1931;1(5):318–333. https://doi.org/10.1063/1.1745010.
43. Paschalis A, Fatichi S, Zscheischler J, et al. Rainfall manipulation experiments as simulated by terrestrial biosphere models: where do we stand? *Glob Chang Biol.* 2020;26(6):3336–3355. https://doi.org/10.1111/gcb.15024.
44. Mastrotheodoros T, Pappas C, Molnar P, et al. More Green and less blue water in the Alps during warmer summers. *Nat Clim Chang.* 2020;10(2):155–161. https://doi.org/10.1038/s41558-019-0676-5.
45. Fatichi S, Leuzinger S, Paschalis A, Langley Adam, Barraclough J, Hovenden AD. MJ. Partitioning direct and indirect effects reveals the response of water-limited ecosystems to elevated CO2. *Proc Natl Acad Sci USA.* 2016;113(45):12757–12762. https://doi.org/10.1073/pnas.1605036113.
46. Zhang Z, Paschalis A, Mijic A. Planning London's Green spaces in an integrated water management approach to enhance future resilience in urban stormwater control. *J Hydrol (Amst).* 2021;597. https://doi.org/10.1016/j.jhydrol.2021.126126.
47. Van Genuchten M.T. *A Closed-Form Equation for Predicting the Hydraulic Conductivity of Unsaturated Soils 1.*; 1980.
48. Tarantino A, Roberts-Self E. Transpiration in the water-limited regime: Soil-plant-atmosphere interactions (EDP Sciences) *E3S Web Conf.* 2023;382. https://doi.org/10.1051/e3sconf/202338213001 (EDP Sciences).
49. Leuning R. Modelling stomatal behaviour and and photosynthesis of eucalyptus grandis. *Funct Plant Biol.* 1990;17:159–175.
50. Carminati A, Vetterlein D, Koebernick N, Blaser S, Weller U, Vogel HJ. Do roots mind the gap? *Plant Soil.* 2013;367(1-2):651–661. https://doi.org/10.1007/s11104-012-1496-9.
51. Robinson EL, Blyth EM, Clark DB, Comyn-Platt E, Rudd AC, Wiggins M. Climate hydrology and ecology research support system meteorology dataset for Great Britain (1961-2019) [CHESS-met] (doi:) *NERC EDS Environ Inf Data Cent (Dataset) Publ Online.* 2023. https://doi.org/10.5285/835a50df-e74f-4bfb-b593-804fd61d5eab.
52. Taborda DMG, Potts DM, Zdravković L. On the assessment of energy dissipated through hysteresis in finite element analysis. *Comput Geotech.* 2016;71:180–194. https://doi.org/10.1016/j.compgeo.2015.09.001.
53. Taborda DMG, Kontoe S, Tsiampousi A. *IC MAGE UMIP - universal model interface for PLAXIS (Version 3.5). Zenodo.* Published online; 2023.
54. Taborda DMG, Kontoe S, Tsiampousi A. *IC MAGE model 01 - strain-hardening/softening Mohr-Coulomb failure criterion with isotropic small strain stiffness (Version 2.1). Zenodo.* Published online; 2023.
55. Alonso E.E., Olivella ' S. *Unsaturated Soil Mechanics Applied To Geoiechnical Problems.*; 2006.
56. Tsiampousi A, Zdravković L, Potts DM. A new hvorslev surface for critical state type unsaturated and saturated constitutive models. *Comput Geotech.* 2013;48:156–166. https://doi.org/10.1016/j.compgeo.2012.09.010.
57. Taborda DMG, Tsiampousi A, Kontoe S. *IC MAGE flow model 02 - Stress-dependent anisotropic permeability (1.0). Zenodo.* Published online; 2023.
58. Kovacevic N., Higgins K.G., Potts D.M., Vaughan P.R. *Undrained Behaviour of Brecciated Upper Lias Clay at Empingham Dam.* Vol 57.; 2007.

59. Wongsaroj J, Soga K, Mair RJ. Tunnelling-induced consolidation settlements in London clay. *Geotechnique*. 2013;63(13):1103–1115. https://doi.org/10.1680/geot.12.P.126.
60. Vaughan PR. Assumption, prediction and reality in geotechnical engineering. *Grotechnique*. 1994;44(4):573–609.
61. Nyambayo VP, Potts DM. Numerical simulation of evapotranspiration using a root water uptake model. *Comput Geotech*. 2010;37(1-2):175–186. https://doi.org/10.1016/j.compgeo.2009.08.008.
62. Potts DM, Zdravkovic L. Accounting for partial material factors in numerical analysis. *Geotechnique*. 2012;62(12):1053–1065. https://doi.org/10.1680/geot.11.P.057.
63. Tsiampousi A, Zdravković L, Potts DM. Variation with time of the factor of safety of slopes excavated in unsaturated soils. *Comput Geotech*. 2013;48:167–178. https://doi.org/10.1016/j.compgeo.2012.08.005.
64. Smethurst JA, Briggs KM, Powrie W, Ridley A, Butcher DJE. Mechanical and hydrological impacts of tree removal on a clay fill railway embankment. *Geotechnique*. 2015;65(11):869–882. https://doi.org/10.1680/jgeot.14.P.010.
65. UKCP. Accessed November 6, 2024. ⟨https://www.metoffice.gov.uk/research/approach/collaboration/ukcp/about/what-is-ukcp⟩.
66. RCP Scenario data group. Accessed November 6, 2024. ⟨https://www.pik-potsdam.de/~mmalte/rcps/⟩.
67. Meinshausen M, Smith SJ, Calvin K, et al. The RCP greenhouse gas concentrations and their extensions from 1765 to 2300. *Clim Change*. 2011;109(1):213–241. https://doi.org/10.1007/s10584-011-0156-z.
68. UKCP18. Convection-Permitting model projections for the UK at 2.2km resolution. Accessed 15 August 2024 *CEDA Arch*; 2024. ⟨https://catalogue.ceda.ac.uk/uuid/ad2ac0ddd3f34210b0d6e19bfc335539/⟩.
69. Riahi K, Grübler A, Nakicenovic N. Scenarios of long-term socio-economic and environmental development under climate stabilization. *Technol Forecast Soc Change*. 2007;74(7):887–935. https://doi.org/10.1016/j.techfore.2006.05.026.